Research Article Vol. 4, No. 1 / 15 Jan 2025 / Optics Continuum 1
OPTICS CONTINUUM

One-dimensional temperature measurement of supersonic jet flow by resonantly ionized photoemission thermometry of molecular nitrogen

ALEKSANDER CLARK, WALKER MCCORD, KYLE PRIDE, AND ZHILI ZHANG

Dept. of Mechanical, Aerospace and Biomedical Engineering, University of Tennessee, Knoxville, TN 37996, USA

Abstract: As the field of fluid dynamics progresses, the demand for sophisticated diagnostic methods to accurately assess flow conditions rises. In this work, resonantly ionized photoemission thermometry (RIPT) has been used to directly target and ionize diatomic nitrogen (N_2) to measure one-dimensional (1D) temperature profiles in a supersonic jet flow. This technique can be considered non-intrusive as the premise uses resonantly enhanced multiphoton ionization (REMPI) to target molecular nitrogen. This resonance excites N_2 into absorption bands of the P, Q, and R rotational branches of N_2 ($b^1\Pi_u$). The ideal (3 + 1) REMPI scheme excites from the ground state and ionizes N_2 ($b^1\Pi_u \leftarrow X^1\Sigma_g^+$) where de-excitation results in photoemission from the first negative band of ionized $N_2^+(B^2\Sigma_u^+ \rightarrow X^2\Sigma_g^+)$ as nitrogen returns to the ground state. The resulting emission can be observed using an intensified camera, thus permitting inference of the rotational temperature of ground-state molecular nitrogen. A linearly regressive Boltzmann distribution is applied based on previous calibration data for this technique to quantify the temperature along the ionized line. This work applies this technique to a pure N_2 supersonic jet in cross-flow and counter-flow orientations to demonstrate N_2 RIPT's applications in a supersonic flow. Temperature variations are observed at different locations downstream of the exit in cross-flow, and axisymmetric in counter-flow, to generate profiles characterizing the flow dynamics. Due to the collisional effects resulting from the number density of N_2 at higher pressures, a (3 + 2) REMPI scheme is observed throughout this text.

1. Introduction

As the field of fluid dynamics continues to evolve, there is an increasing need for advanced diagnostic techniques that can precisely analyze flow conditions. Flow temperatures in supersonic flows are of significant interest, which give insight into how energy is distributed and dissipated [1–3]. Additionally, these measurements help to improve computational modeling of supersonic flows by providing calibration data sets. Non-intrusive optical diagnostic techniques are best suited as perturbations of the flow are kept to a minimum. The use of lasers is a popular approach as flow perturbing hardware, such as pitot tubes and thermocouples, are not needed. A laser beam can be directed and tailored to achieve results specific to the experiment. Examples of other laser-based temperature measurement techniques are coherent anti-Stokes Raman scattering (CARS) [4–6] and planar laser induced fluorescence (PLIF) [7–11]. CARS presents accurate point temperature measurements in supersonic flows, although this can be difficult to align and execute depending on the experimental parameters and environments. PLIF gives a two-dimensional planar temperature profile, though in most cases needs a tracer to be seeded into the flow potentially changing some of the fluid characteristics.

#543309 https://doi.org/10.1364/OPTCON.543309
Journal © 2025 Received 25 Sep 2024; revised 13 Nov 2024; accepted 14 Nov 2024; published 16 Dec 2024

OPTICS CONTINUUM

Molecular oxygen-based resonantly ionized photoemission thermometry (O_2 RIPT) [12–14] can accurately determine the temperature of air along a one-dimensional fluoresced line. In O2 RIPT, molecular oxygen is resonantly ionized by (2 + 1) resonance enhanced multi-photon ionization (REMPI). The same laser pulse produces avalanche ionization of molecular nitrogen, N_2^+, present in air. The fluorescent emissions of the first negative band of N_2^+ can be used to quantify the molecular oxygen REMPI processes, which is directly proportional to the rotational temperatures of the flow [15–18].

Similarly, N_2 RIPT resonantly ionizes nitrogen molecules in air thus producing the fluorescent emissions from the first negative band of N_2^+ like with O_2 RIPT [19–21]. The main difference between the two is N_2 RIPT directly excites N_2 without the need for an O_2 intermediate. Using the fluorescent emission intensities, a Boltzmann analysis is performed, and a rotational temperature is obtained. The measurement is typically with an error of less than 5% for temperatures not exceeding 600 Kelvin. Since N_2 molecules are naturally existent in air, there is no need to seed a tracer to induce fluorescence as in PLIF. Previous experiments explored the dependency between fluorescence intensity and temperature to establish calibration excitation schemes. The fluorescent signal produced from each resonant line for a given temperature can be plotted according to an equilibrium Boltzmann distribution thus relating the local rotational temperatures.

Here N_2 RIPT was used to measure the one-dimensional temperature profile in an under-expanded supersonic flow from a nozzle with nominal design of Mach 1. [22–24] A (3 + 2) REMPI scheme of molecular nitrogen was used to produce emissions in the first negative band of ionized molecular nitrogen. The laser was oriented perpendicular to the supersonic flow for crossflow temperature measurements at various points along the flow path. Subsequently, the laser beam was directed to counter-propagate along the supersonic jet flow, enabling counter flow temperature measurements to achieve a line-wise assessment. The measurements have good agreements for both configurations. The applications performed show the capability of N_2 RIPT to capture the temperature variations at different points along a line in the supersonic jet flows.

2. Theoretical background

Resonance-enhanced multiphoton ionization (REMPI) [18,19] is implemented to excite molecular nitrogen in the supersonic jet flow. A (3 + 1) REMPI scheme is used to ionize N_2 by first exciting molecular nitrogen to an intermediate state with three photons, then an additional photon is absorbed to ionize. Standard atmospheric pressure increases collisions that may occur resulting in an additional photon needed for ionization. This becomes a (3 + 2) REMPI scheme to compensate for the collisional losses. The previous publications [12,19] outline in detail the fundamental process of the RIPT technique for O_2 and N_2. For coherency of this paper, some of the mechanisms in the technique will be discussed for the application of N_2.

The targeted transition is $N_2(X^1\Sigma_g^+, v = 0 \rightarrow b^1\Pi_u, v = 6)$ absorption band [25]. The recombination of the electrons and nitrogen molecules results in observable fluorescent emissions. The emissions resulting are in the first negative band of $N_2^+(B^2\Sigma_u^+ – X^2\Sigma_g^+)$, specifically 390 nm ($\Delta v_0; 1 \rightarrow 0$) and 430 nm ($\Delta v_1; 1 \rightarrow 1$) transitions. The absorptive wavelengths were chosen from previous experiments to have the strongest fluorescent emissions dependent on temperature.

The N_2 RIPT (3 + 2) REMPI scheme has a two-step mechanism in the ionization of N_2. First, the (3 + 2) REMPI for molecular nitrogen excitation which ionizes to N_2^+, as described by Eq. (1).

$$N_2 + 5h\nu_{REMPI} \rightarrow N_2^+ + e^- \tag{1}$$

where $h\nu_{REMPI}$ is absorbed photons by REMPI and e^- is the free electron from photoionization.

Second, the recombination of free electrons and molecular nitrogen ions resulting in spectral emissions in the first negative and first positive bands, as described by Eqs. (2) and (3), respectively.

$$N_2^+(B) \rightarrow N_2^+(X) + \hbar\nu_{1^-} \tag{2}$$

OPTICS CONTINUUM

$$N_2^+ + e^- \rightarrow N_2(B) \rightarrow N_2(A) + \hbar\nu_{1^+} \tag{3}$$

where $\hbar\nu_1^-$ is the first negative emissions of the molecular nitrogen ion, and $\hbar\nu_1^+$ is the first positive emissions of molecular nitrogen.

The resulting lifetime of the targeted first negative band, as outlined in [26], is on the order of 10^{-8} seconds, which is ideal for temperature studies as longer lifetimes could adversely affect the photoemission rotational state and temperature dependence. The short lifetime of the first negative emissions is a result of low energy deposition into the flow resulting in only rotational energy changes.

The temperature can be determined from the images taken by converting the intensity to a signal and creating a linear fit among the wavelengths associated with the temperature calibration shown in [18]. The resulting slope is the inverse negative proportional to the signal and energy states, shown in Eq. (4).

$$-\frac{1}{k_B T} \propto \ln\left(\frac{I_{\lambda_n}}{S(J', J')}\right) / E_{g_n} \tag{4}$$

where, k_B is the Boltzmann constant, $S(J', J')$ is the transitional line strength, E_{g_n} the ground state energy, I_{λ_n} the signal intensity of the imaged wavelength, and T the medium temperature to be solved for. The subscript n denotes the corresponding intensity and ground state energy respective to each targeted resonance wavelength. This Boltzmann distribution will be the statistical mechanism that allows for a temperature measurement based on the signal intensity provided through imaging [19,25].

Using isentropic flow relations for a Mach 1 air jet, the approximate temperature can be determined at the nozzle exit. [22–24] This leads to the selection of the proper excitation wavelengths based on their associated best fit temperature. Table 1 shows two possible options for the associated temperature calibration obtained experimentally from varying air temperature and probing with select calculated rotational excitation wavelengths. Since isentropic flow relations state that exit temperature T_e < stagnation temperature T_0, where T_0 is approximately 293 K, all tabulated excitation wavelengths were used to probe the flow. Noted, there is a higher error percentage for the excitation wavelengths associated with the 230 K calibration. This can be attributed to a poor SNR relating to cooler temperatures at standard atmospheric pressure. Applications within low pressure, thus low number density regions, are expected to have an improved SNR.

Table 1. N_2 Resonance Wavelengths Used and Potential Temperature Errors

N_2 Excitation Wavelengths (nm)				Actual Temperature (K)	Measured Temperature (K)	Error (%)
284.712	284.726	284.748	284.798	230	242	5.22
284.712	284.879	284.940	285.031	293	292	0.34

3. Experimental setup

Supersonic flow was produced by an air jet with a nominal Mach 1 geometry, whose working fluid for this experiment was ultra-high purity nitrogen [27]. The nitrogen flowed through a two-stage high-flow regulator to maintain pressure while the jet was active. The pressure prior to jet startup was set to 0.345 MPa gauge (50 psig). A pressure gauge was located just before the stagnation point of the nozzle. During the experiment, the gauge readout was 0.296 MPa gauge (43 psig). At this pressure an under-expanded supersonic jet was produced for resonance probing and temperature analysis of the shock structures.

OPTICS CONTINUUM

3.1. N_2 resonant wavelength laser beam generation

To generate the resonance wavelengths necessary to excite N_2, a Continuum Nd:YAG nanosecond laser was used. The laser operated at 10 Hz with a pulse width of 10 ns. The 532 nm second harmonic of the Nd:YAG was targeted for this experiment. The laser energy maintained at 532 nm was approximately 220 millijoules per pulse. The laser beam was pumped into a Continuum ND6000 dye laser equipped with a grating of 1800 lines/mm to shift the wavelength to a tunable range between 569 nm and 571 nm with a linewidth of 0.01 nm. This was accomplished with a mixture of rhodamine 6 G perchlorate and rhodamine 610 perchlorate dye reagents. The laser energy output after optimizing the dye concentrations in ND6000 was approximately 58 mJ/pulse. Finally, the tunable wavelength was pumped into a Continuum UVT frequency doubling module generating wavelengths between 284.50 nm and 285.50 nm. The output wavelengths for this experiment were verified via a xenon lamp calibrated spectrometer and fine-tuned to maximum energy and fluorescence to verify the known target resonance peak was achieved. The final ultra-violet (UV) laser energy output was maintained at 9.0 ± 0.1 mJ/pulse at each targeted resonance peak.

3.2. Supersonic jet cross flow and counter flow configurations

The tuned UV beam was focused using a fused silica lens with an effective focal length (EFL) of 200 mm. This lens was selected based on the fluorescent line length written within the confocal region of the focused beam, and the signal to noise ratio (SNR) of the images captured. Depending on the targeted resonance wavelength and generated fluorescence, the observable written line was between 1 to 2 cm. The parameters just discussed were done in preliminary tests performed for the N_2 RIPT calibration using the same equipment as described in [19]. A Princeton Instruments PI-Max 4 ICCD intensified camera was used to capture the tagged flow the moment it was fluoresced by the focused resonant beam. The camera gate and laser pulse were synchronized via a Stanford Research Systems DG645 delay generator.

A photodiode was used to capture the beam pulse at the exit of the UVT and generate a signal to be monitored. An oscilloscope was used to verify synchronization of the camera gate, via a monitor output on the camera, and laser pulse, via the photodiode. A Schott BG-3 bandpass filter was used to capture the first negative and first postive emissions of the N_2 deexcitation process eliminating scattering from the dye laser. The BG-3 has a transmission greater than 80% for approximately 300-425 nm, and 750-1000 nm, but only the prompt fluorescence of the first negative band in the UV range was captured since the CCD on the PI-Max used has low quantum efficiency in the NIR and IR range. Figures 1(i) and 1(ii) show the cross flow and counter flow experimental setups respectively.

Both crossflow and counterflow configurations used a three-axis translation stage for positioning the jet. For the crossflow setup, the x-z plane was used to position the jet just beneath the center of the resonantly generated line. The y axis was used to adjust the jet vertically to probe different locations downstream of the jet. This resulted in multiple measurements with a fluorescent line perpendicular to the supersonic flow. The counterflow configuration positioned the jet on the y-z plane so that the jet exit was aligned with the resonantly generated line. The jet was adjusted along the x axis so that the strongest fluorescent line terminated at the nozzle exit, maximizing the distance captured in the supersonic flow.

The intensified camera was set to capture 20 successive images for each of the resonance lines in all positions for cross flow and counter flow. A gate width of 30 ns was used to capture the full lifetime of the prompt fluorescence in each image. The camera gate synchronization with the 10 Hz pulse rate of the laser resulted in a 2 second capture time for each resonant wavelength. The number of images captured was chosen and used to improve the SNR in post process averaging, which was determined from preliminary tests already discussed.

OPTICS CONTINUUM

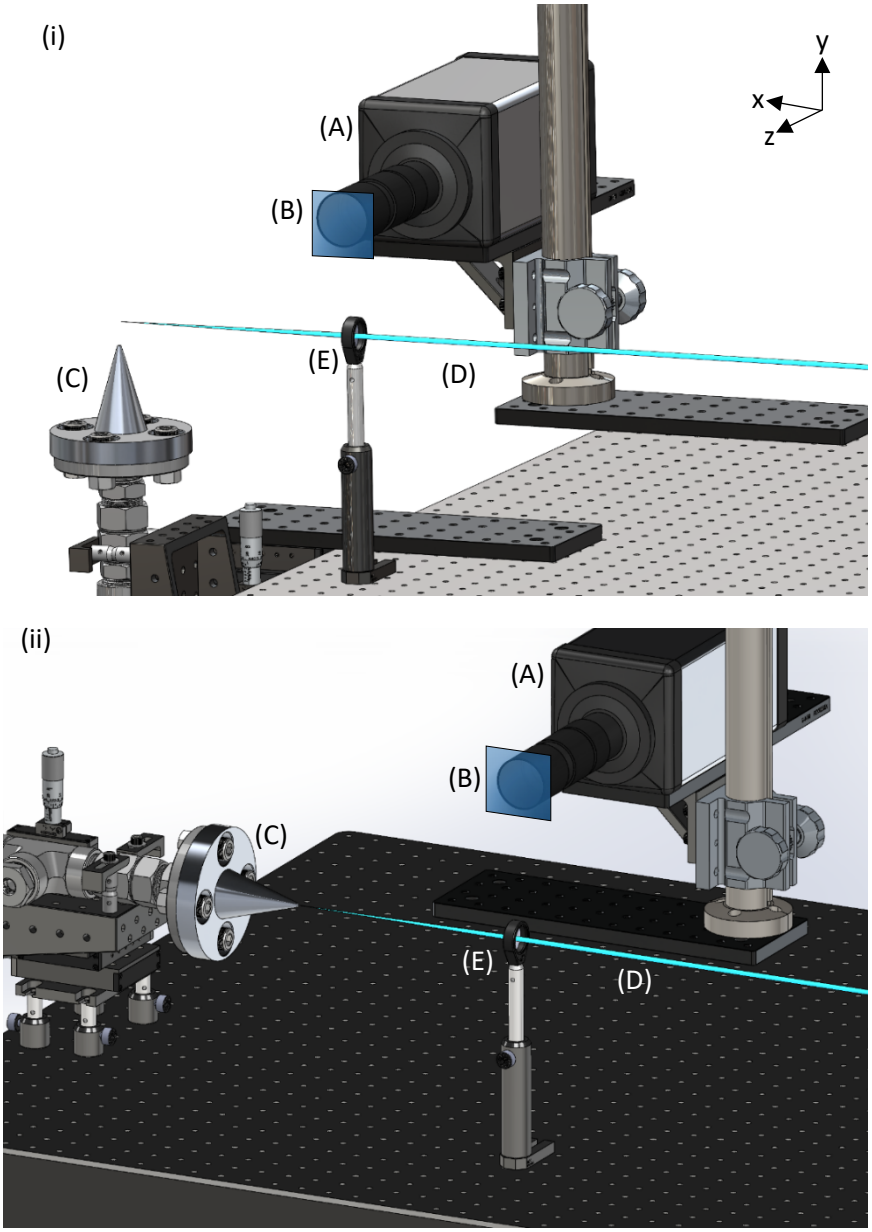

Fig. 1. (i) Mach 1 nozzle crossflow configuration and (ii) counterflow configuration. The configuration includes (A) Intensified camera, (B) bandpass filter, (C) Mach 1 nozzle, (D) resonant laser beam, and (E) focusing lens.

OPTICS CONTINUUM

4. Results and discussions

For each of the resonance lines, the average of the 20 images was taken, thus assigning a mean intensity value for each of the pixels in the 512×512 image produced. Only relevant photoemission captured by the camera was focused on. Irrelevant background was cropped away leaving the desired region of interest (ROI). The remaining background within the ROI was filtered to remove any artifacts while maintaining the integrity of the relevant photoemission information. The filter used a mask that targeted intensity values great enough to be fluorescence and forced the remaining low intensity artifact values to zero. It was possible to differentiate between the fluorescence and artifacts due to the large intensity difference between the two. The mean of the entire ROI was taken along the axis parallel to the emission line, thus refining the intensity value assigned to each of the pixels along a one-dimensional line. The intensity captured by the camera was converted into a signal described by the numerator of Eq. (4).

Using Eq. (4), taking the negative inverse slope of the linear line fit yields the temperature multiplied by the Boltzmann constant. Thus, dividing by the constant, the temperature is calculated for a single differential length equal to the pixel size. Doing this for all pixels along the line yields the one-dimensional temperature distribution. A correction factor is applied to the linear regression after solving for temperature in Eq. (4) and is a small multiplicity of the inverse slope. A correction of 5% greater than the uncorrected value was used in these experiments. This correction factor is relative to the experimental setup, namely the laser being used. This is due to the nonlinear relationship between laser power and the fluorescent intensity observed.

After scanning across all resonant wavelengths listed in Table 1 for both configurations of crossflow and counterflow, each of the signals were plotted against their respective ground state energy, per resonant wavelength, along a 1-D line and four were selected for a linearly regressive best fit along a Boltzmann distribution. Table 2 lists the four resonant lines that met this criterion for this experimental setup and temperature regime. The corresponding correction factor was calculated based on the known ambient temperature outside the supersonic flow in the crossflow configuration. In this experiment, the known temperature was the ambient room temperature outside the jet stream at 293 K. This was possible since the fluorescent line observed was longer than the effective diameter of the supersonic flow.

Table 2. Revised N_2 Resonance Wavelengths for a Supersonic Jet

N_2 Excitation Wavelengths (nm)				Configuration	Average R^2	St. Dev.
284.712	284.798	284.940	285.031	Crossflow	0.884	0.034
				Counterflow	0.905	0.017

Supplement 1 shows the computation fluid dynamics (CFD) of the supersonic jet under ideal conditions using the same running pressure noted in these experiments. The CFD was computed with air, rather than N_2, so there is some variation in the results. It does however show that T_e and temperature in the first shock diamond are consistent with the experimental results. Other variations between the data downstream are likely due to environmental factors such as imperfections in the nozzle geometry. Since the CFD is a simulation of ideal temperatures, fluorescence variations within the averaged images has an impact on the resulting temperature profiles obtained.

4.1. Crossflow

Six points of interest were chosen to probe with N_2 resonance along the supersonic flow path. These points are identified in Fig. 2, which shows a Schlieren image of the Mach 1 jet at the operating conditions previously mentioned. The X/X_D is the ratio of downstream distance of

OPTICS CONTINUUM

the nozzle exit to nozzle exit diameter, of which is 0.125 inches. These points were chosen to measure the temperature in the different shock regions of the shock train.

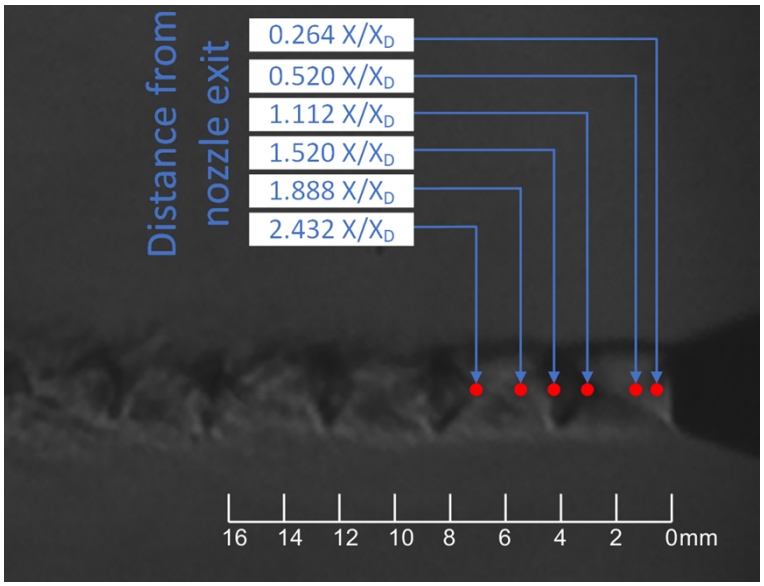

Fig. 2. Schlieren image of the crossflow measurement locations for the Mach 1 nozzle at 0.345 MPa gauge (50 psig) pre-startup stagnation pressure.

Density changes of the RIPT technique have been shown to have little effect on the Boltzmann distribution as it relates to temperature if the flow conditions are constant, thus densities are assumed the same for each corresponding data point in the linear regression model of the distribution [12,19]. This assumption does introduce some errors and is discussed later in the text. A final raw temperature profile for all the probed positions is shown in Fig. 3. For visual comparison, Fig. 4 shows the intensity of the emissions as captured by the intensified camera. Isentropic flow calculations based on the stagnation temperature for the Mach 1 nozzle put the T_e at 244 Kelvin, but due to limitations in acquiring the prompt fluorescence with the filter used, scattering from the nozzle exit overpower the signal. For this experiment the axis has been turned for crossflow and thus the distances from the nozzle are reported in y/D, corresponding to the axes in Fig. 1. It is important to note that the observed intensities for each resonance line do not correlate directly to a temperature since they are relative to the focused laser energy distribution in the fluorescent region. Instead, each resonance line must be applied in a Boltzmann distribution to calculate the temperature, as discussed previously.

A correction factor for the solving for the temperature was calculated using a known temperature that is present in the images. Since the fluorescence captured by the camera was 1 to 2 cm in length and the nozzle exit was 0.32 cm in diameter, the supersonic jet had a more drastic impact on the fluoresced intensity where present. The “tails” of the fluorescence were assumed to be room temperature, thus a correction factor was calculated and applied. Even though the jet was assumed to have a symmetrical flow, density variations can be seen in the cross-section emission with higher densities likely on the right side of the axis. This introduces some error, previously mentioned, and is noted by the standard deviation in Table 3. By focusing on the “tails” that had a higher R^2 value in the linear regression distribuion, the factor could be adjusted to find a mean temperature among the lines’ “tails” at approximately room temperature. Table 3 provides the mean and standard deviations for all lines of the right tail for the lines. Figure 5 shows the R^2 plots across the lines that was the motivation for their selection.

OPTICS CONTINUUM

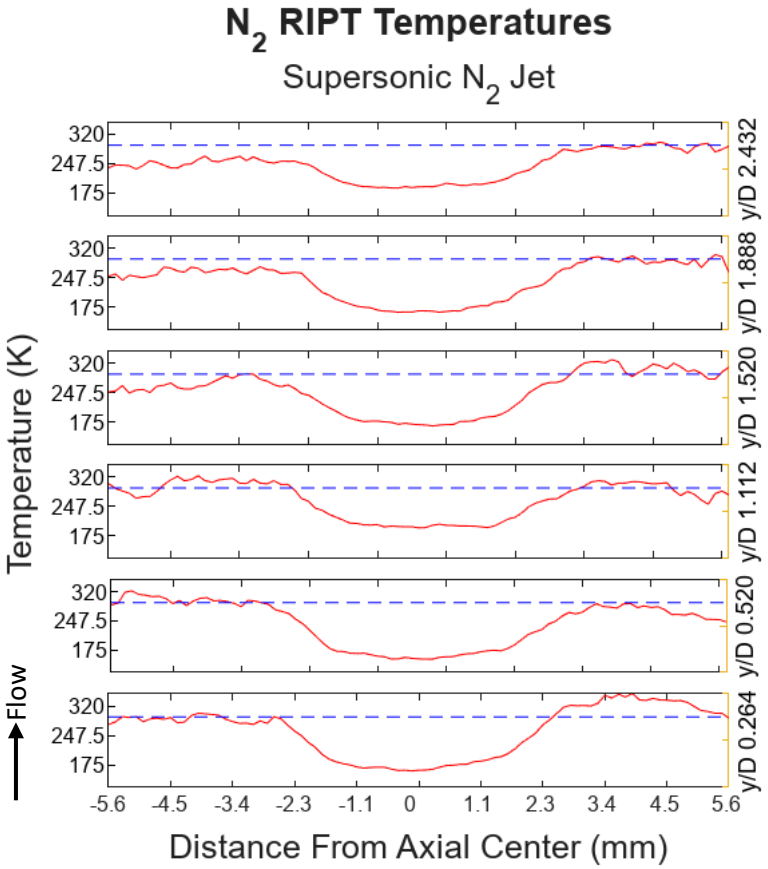

Fig. 3. Temperature profile for each of the crossflow measurements with N_2 resonance in a supersonic air jet. The blue dotted line denotes room temperature at 293 Kelvin.

Table 3. Mean and Standard Deviation of Line (Right Tail) Temperatures

Jet position [x/D]	Mean Temperature [K]	Standard Deviation [K]
2.432	327.7	7.14
1.888	271.8	10.2
1.520	292.3	14.2
1.112	306.2	17.3
0.520	288.4	14.8
0.264	289.2	17.3
All Lines	295.9	19.0

OPTICS CONTINUUM

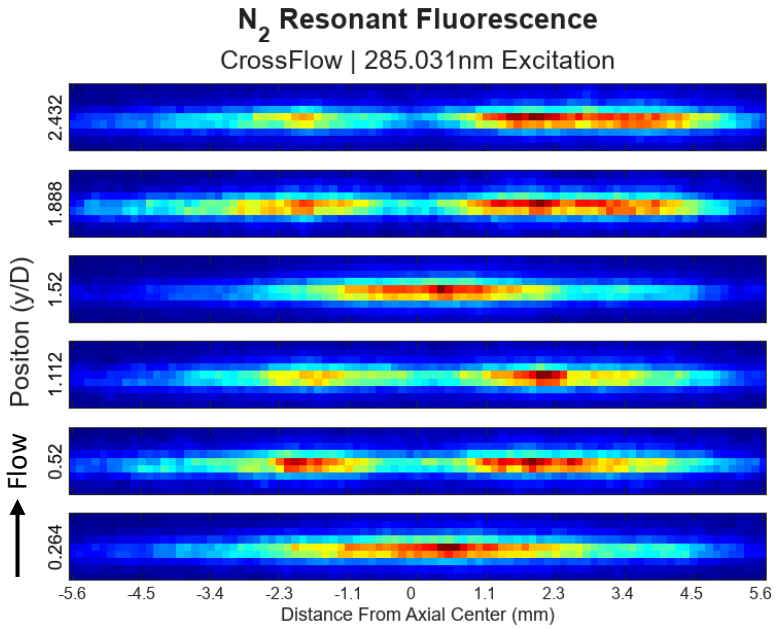

Fig. 4. Images of the first negative emission of nitrogen with 285.031 nm resonance of a pure N_2 jet. The images shown are the direct imaging capture of the various crossflow locations by the ICCD camera with a band pass filter targeted for the first negative emissions of nitrogen.

4.2. Counterflow

The resonant wavelength laser beam was aligned with anti-parallel propagation against the supersonic jet flow. The beam was focused through the center of the jet flow to capture assumed axisymmetric shock variations. The nozzle and fluorescent emission line were positioned so that one of the ends of the emission line was just inside the nozzle. The "tail" of the ionized line was small enough with a low enough energy to avoid high energy breakdowns on the nozzle exit as well as most reflective scattering. Remaining reflective scattering was reduced with light absorptive paint.

The temperature was calculated as before by plotting the signals, captured from the intensities captured, against the ground state energy of their respective resonance wavelengths. The linear regression fit was applied, and the correction factor calculated from the crossflow was applied. The temperature distribution of the counterflow configuration is shown in Fig. 6. Also shown in Fig. 6 is the point relative minima and maxima of the calculated error, excluding outliers. Clearly seen along the distribution are the shock structures present in an under-expanded jet. This shows the impact of compressible effects on the temperature at the various locations through the center of an assumed axisymmetric shock train. Figure 7 shows the intensity of each fluoresced line captured by the camera.

The most noticeable observation when comparing the fluorescence from the four excitation wavelengths is the intensity disparity between the two lower wavelengths and the two higher wavelengths. This is a result of the necessity to use resonance wavelengths sampled from both the 230 Kelvin and the 293 Kelvin calibration temperatures and results. Figure 8 shows the quality of the linear regression fit with a lower R^2 near the nozzle exit due to low intensity of the fluorescence captured, but still returns a recoverable temperature previously shown.

OPTICS CONTINUUM

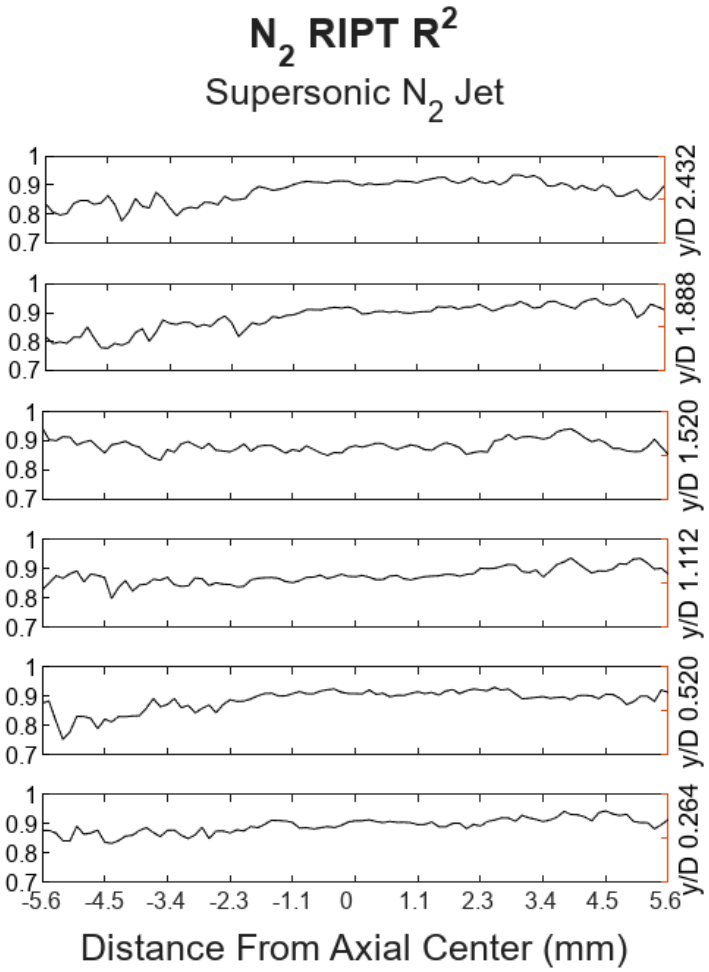

Fig. 5. Linear R^2 fit of the Boltzmann distribution for each probed position of the pure N_2 supersonic jet.

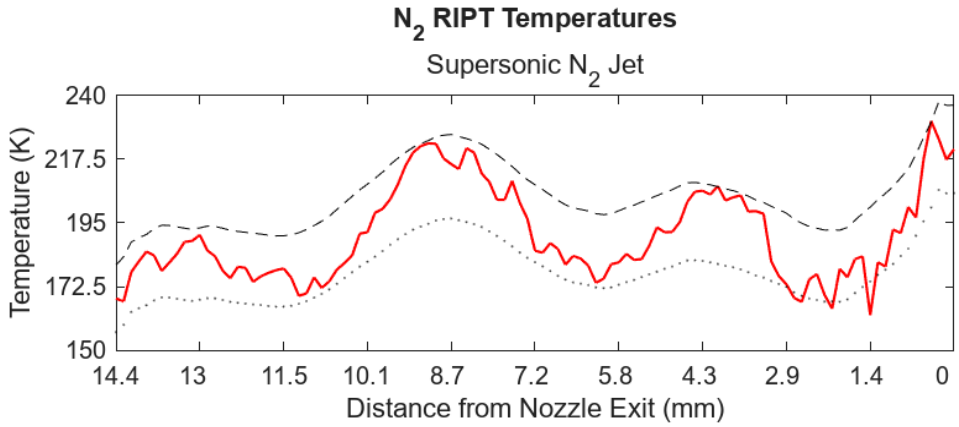

Fig. 6. Temperature distribution of an under-expanded jet using N_2 RIPT. Flow is from right to left. Dashed line represents approximate upper limit of error. Dotted line represented approximate lower limit of error.

OPTICS CONTINUUM

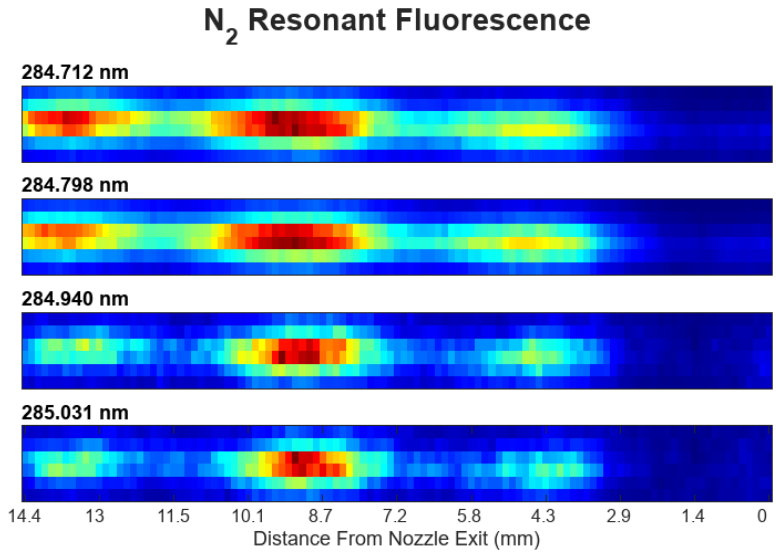

Fig. 7. Emission fluorescence of the chosen N_2 excitation lines for the counterflow experiment. The nozzle exit is at 0 mm; flow is from right to left.

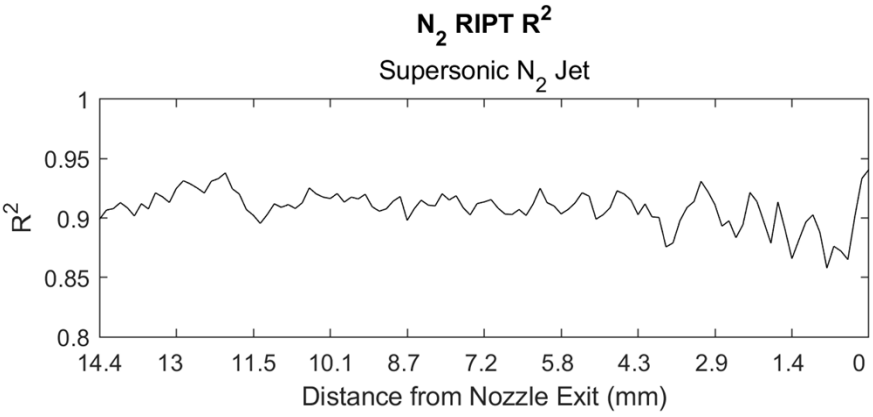

Fig. 8. R^2 of the linear fit for the chosen excitation lines on the Boltzmann distribution.

OPTICS CONTINUUM

5. Conclusions

In this series of experiments, temperature profile in a supersonic jet flow was measured by Resonantly Ionized Photoemission Thermometry of molecular nitrogen (N_2 RIPT). By utilizing multiple excitation lines, the emission is strong enough to be directly captured by an intensified scientific camera. Rotational temperature of N_2 molecules was obtained from the emissions by a linear regression fit applied to the Boltzmann distribution of molecular nitrogen at the ground states. for a time resolved temperature measurement of the supersonic flow. Two configurations for the supersonic flow were specifically tested:

Crossflow orientation shows temperature variations at different locations along the flow path to gather data across the entire flow structure at that point. Because the RIPT measurement is a one-dimensional line, the shock interactions within the flow structure can be captured like looking at a cross section of the temperature profile across the flow region. The different locations are selected to show varying flow characteristics present in an under-expanded supersonic jet.

Counterflow orientation relies on a single measurement at the axisymmetric center of the supersonic flow. The 1D RIPT line written in the flow captures the temperature characteristics of the shock interactions directly in the center of the flow. This measurement shows the temperature variations in the direction of the flow at more flow path points than that of crossflow.

The results of these experiments show that the N_2 RIPT technique can be applied to a supersonic jet with moderate accuracy. It can also be seen that the excitation wavelengths are dependent on the nature of the experiment, thus a correction factor must be found and accounted for. It can also be noted that the correction factor, though dependent on the excitation wavelengths, is constant for those wavelengths observed with the same equipment. Further validation for the calibration technique used here was that there was good agreement in the temperature distribution between the crossflow and counterflow using the same correction factor calculated from the crossflow data.

Based on this, the experiments outlined here have an error of approximately 7% on average, referencing the edges of the crossflow data compared to room temperature, which is slightly higher than previously mentioned for the calibration resonant lines and temperatures from previous experiments. The technique can be applied with very little experimental calibration so long as a baseline is known, as such with the case of the crossflow results that were outlined.

Future applications of this technique can be applied to wind tunnels that use air or pure nitrogen so that temperatures can be measured across shocks from varying geometry or to characterize the tunnel flows. This introduces a new method to measure temperature non-intrusively with a simple setup laser and camera setup. Non-intrusive diagnostics techniques become increasingly important as wind tunnels move into higher velocity regimes.

Funding. University of Tennessee, Knoxville; U.S. Department of Energy; Division of Chemical, Bioengineering, Environmental, and Transport Systems (2026242, 2409331).

Acknowledgments. This work is supported by the University of Tennessee, NSF - 2026242, NSF - 2409331 and DOE.

Disclosures. The authors declare no conflicts of interest.

Data availability. Data underlying the results presented in this paper are not publicly available at this time but may be obtained from the authors upon reasonable request.

Supplemental document. See Supplement 1 for supporting content.

References

1. R. Miles, A. Dogariu, and L. Dogariu, "Localized time accurate sampling of nonequilibrium and unsteady hypersonic flows: methods and horizons," Exp. Fluids **62**(12), 248 (2021).
2. P.M. Danehy, R. A. Burns, D. T. Reese, *et al.*, "FLEET velocimetry for aerodynamics," Annu. Rev. Fluid Mech. **54**(1), 525–553 (2022).
3. S.W. Grib, N. Jiang, P. S. Hsu, *et al.*, "Rayleigh-scattering-based two-dimensional temperature measurement at 100-kHz frequency in a reacting flow," Opt. Express **27**(20), 27902–27916 (2019).

OPTICS CONTINUUM

4. J. Kuhfeld, N D Lepikhin, D Luggenhölscher, *et al.*, "Vibrational CARS measurements in a near-atmospheric pressure plasma jet in nitrogen: I. Measurement procedure and results," J. Phys. D: Appl. Phys. **54**(30), 305204 (2021).
5. A. Hosseinnia, M. Ruchkina, P. Ding, *et al.*, "Single-shot fs/ns rotational CARS for temporally and spectrally resolved gas-phase diagnostics," Proc. Combust. Inst. **38**(1), 1843–1850 (2021).
6. A. Dogariu, "Velocity and temperature measurements in mach 18 nitrogen flow at tunnel 9," in *AIAA Scitech 2021 Forum*. 2021, American Institute of Aeronautics and Astronautics.
7. S.A. Skeen, J. Manin, and L.M. Pickett, "Simultaneous formaldehyde PLIF and high-speed schlieren imaging for ignition visualization in high-pressure spray flames," Proc. Combust. Inst. **35**(3), 3167–3174 (2015).
8. L.K. Su and N.T. Clemens, "Planar measurements of the full three-dimensional scalar dissipation rate in gas-phase turbulent flows," Exp. Fluids **27**(6), 507–521 (1999).
9. M. Gragston, J. Sawyer, S. F. Adams, *et al.*, "Radar resonance-enhanced multiphoton ionization for measurement of atomic oxygen in non-equilibrium pulsed plasmas," J. Appl. Phys. **125**(20), 203301 (2019).
10. P. Danehy, "Non-intrusive measurement techniques for flow characterization of hypersonic wind tunnels," 2018.
11. P.M. Danehy, S. O'Byrne, A. Frank, *et al.*, "Flow-tagging velocimetry for hypersonic flows using fluorescence of nitric oxide," AIAA J. **41**(2), 263–271 (2003).
12. W. McCord, A. Clark, and Z. Zhang, "One-dimensional air temperature measurements by air resonance enhanced multiphoton Ionization thermometry (ART)," Opt. Express **30**(11), 18539–18551 (2022).
13. W. McCord, A. M. Clark, Z. Zhang, *et al.*, "One-dimensional resonantly ionized photoelectron thermometry measurements in supersonic flow around a cylinder," in *AIAA SCITECH 2023 Forum.* 2023.
14. W. McCord, A. Clark, and Z. Zhang, "1D temperature measurements by air REMPI thermometry (ART)," in *AIAA SCITECH 2022 Forum.* 2022.
15. Y. Wu, M. Gragston, Z. Zhang, *et al.*, "Spatially localized, see-through-wall temperature measurements in a flow reactor using radar REMPI," Opt. Lett. **42**(1), 53–56 (2017).
16. Y. Wu, M. Gragston, and Z. Zhang, "Acoustic detection of resonance-enhanced multiphoton ionization for spatially resolved temperature measurement," Opt. Lett. **42**(17), 3415–3418 (2017).
17. Y. Wu, Z. Zhang, and S.F. Adams, "Temperature sensitivity of molecular oxygen resonant-enhanced multiphoton ionization spectra involving the C 3 Π g intermediate state," Appl. Phys. B **122**, 1–10 (2016).
18. Z. Zhang, M.N. Shneider, and R.B. Miles, "Coherent microwave scattering from resonance enhanced multi-photon ionization (radar REMPI): a review," Plasma Sources Science and Technology **30**(10), 103001 (2021).
19. W. McCord, A. Clark, and Z. Zhang, "One dimensional temperature measurements by resonantly ionized photoemission thermometry of molecular nitrogen," Optics Continuum **2**(11), 2255–2269 (2023).
20. W. McCord, A.M. Clark, and Z. Zhang, "One-Dimensional Nitrogen-based Resonantly Ionized Photoelectron Thermometry (N2 RIPT)," in *AIAA SCITECH 2023 Forum.* 2023.
21. A.M. Clark, W. McCord, K. Pride, *et al.*, "1D temperature measurement of a supersonic air jet with N2 resonantly ionized photoemission thermometry," in *AIAA SCITECH 2023 Forum.* 2023.
22. T.C. Adamson and J.A. Nicholls, "On the structure of jets from highly underexpanded nozzles into still air," Journal of the Aerospace sciences **26**(1), 16–24 (1959).
23. P. Behrouzi and J.J. McGuirk, "Underexpanded jet development from a rectangular nozzle with aft-deck," AIAA J. **53**(5), 1287–1298 (2015).
24. E. Franquet, V. Perrier, S. Gibout, *et al.*, "Free underexpanded jets in a quiescent medium: A review," Prog. Aeronaut. Sci. **77**, 25–53 (2015).
25. S. Adams and J. Williamson, "Spectroscopic study of N2(b(1)Πu, v=8) by atmospheric pressure resonant-enhanced multiphoton ionization and fluorescence detection," The journal of physical chemistry. A **117**(1), 1 (2013).
26. A. Lofthus and P.H. Krupenie, "The spectrum of molecular nitrogen," J. Phys. Chem. Ref. Data **6**(1), 113–307 (1977).
27. P. Cumber, M. Fairweather, S. A. E. G. Falle, *et al.*, "Predictions of the structure of turbulent, highly underexpanded jets," J. Fluids Eng. **117**(4), 599–604 (1995).